Reuniens thalamus recruits recurrent excitation in medial prefrontal cortex.

Gil Vantomme, Gabrielle Devienne, Jacob M Hull, John R Huguenard*

Department of Neurology and Neurological Sciences, Stanford University, Stanford, CA, USA.

Corresponding author: John R Huguenard, Stanford Neuroscience Building S189, 290 Jane Stanford Way, Stanford, CA 94305-5088

Email: huguenard@stanford.edu

Keywords: reuniens, prefrontal cortex, electrophysiology, hippocampus.

Abstract

Medial prefrontal cortex (mPFC) and hippocampus are critical for memory retrieval, decision making and emotional regulation. While ventral CA1 (vCA1) shows direct and reciprocal connections with mPFC, dorsal CA1 (dCA1) forms indirect pathways to mPFC, notably via the thalamic Reuniens nucleus (Re). Neuroanatomical tracing has documented structural connectivity of this indirect pathway through Re however, its functional operation is largely unexplored. Here we used *in vivo* and *in vitro* electrophysiology along with optogenetics to address this question. Whole-cell patch-clamp recordings in acute mouse brain slices revealed both monosynaptic excitatory responses and disynaptic feedforward inhibition for both Re-mPFC and Re-dCA1 pathways. However, we also identified a novel biphasic excitation of mPFC by Re, but not dCA1. These early monosynaptic and late recurrent components are in marked contrast to the primarily feedforward inhibition characteristic of thalamic inputs to neocortex. Local field potential recordings in mPFC brain slices revealed that this biphasic excitation propagates throughout all cortical lamina, with the late excitation specifically enhanced by $GABA_AR$ blockade. *In vivo* Neuropixels recordings in head-fixed awake mice revealed a similar biphasic excitation of mPFC units by Re activation. In summary, Re output produces recurrent feed-forward excitation within mPFC suggesting a potent amplification system in the Re-mPFC network. This may facilitate amplification of dCA1->mPFC signals for which Re acts as the primary conduit, as there is little direct connectivity. In addition, the capacity of mPFC neurons to fire bursts of action potentials in response to Re input suggests that these synapses have a high gain.

Significance statement

The interactions between medial prefrontal cortex and hippocampus are crucial for memory formation and retrieval. Yet, it is still poorly understood how the functional connectivity of direct and indirect pathways underlies these functions. This research explores the synaptic connectivity of the indirect pathway through the Reuniens nucleus of the thalamus using electrophysiological recordings and optogenetic manipulations. The study found that Reuniens stimulation recruits recurrent and long-lasting activity in mPFC - a phenomenon not previously recorded. This recurrent activity might create a temporal window ideal for coincidence detection and be an underlying mechanism for memory formation and retrieval.

Introduction

The direct and indirect pathways between the hippocampus and the medial prefrontal cortex (mPFC) play a significant role in emotional, contextual and spatial processing (1, 2). The direct pathway is generally associated with working memory, learning, and contextual processing (2). The indirect pathways, through intermediary regions like the thalamic Reuniens nucleus (Re), might be important for controlling the amount and type of information retrieved (3). Accumulating evidence suggests that the Re plays a central role in coordinating neuronal activity within the mPFC and hippocampus. Lesions (4) or inhibition (5, 6) of Re reduce coherence between mPFC and hippocampus, in particular in the delta (2-5Hz) and gamma (30-90Hz) frequency ranges. Recently, optogenetic activation of Re was shown to increase mPFC/hippocampus beta (15-30Hz) coherence, which is linked with non-spatial sequence memory (7).

Behaviorally, the Re has been linked to many cognitive processes, most notably: goal directed behavior, working memory, inhibitory control, avoidance and behavioral flexibility (for review (8)). Large efforts have been made in recent years to evaluate the behavioral consequences of permanent lesions, optogenetic manipulation, and pharmacological inhibition of Re in rodents. However, the impact of Re lesions in recognition tasks is controversial. Jung et al. (9) reported a reduction in the exploration time of novel object/displaced object while Barker and Warburton did not observe these changes (10). Lesion of Re led to an increase in performance in some attention dependent tasks (11) but deficits in others (12). Inactivation of Re increased generalization of aversive memory (13) and deficit in the performance in tasks requiring spatial working memory (14) or its encoding (15).

The broad spectrum of functions in which Re is implicated and the disparities observed across these studies, emphasizes the complexity of the indirect pathways between hippocampus and mPFC.

Understanding this network requires an in-depth exploration of the circuit connectivity that underpins its functionality. However, little is known about the synaptic properties, neurotransmitter receptor content, plasticity profile or synaptic integration at the Re-mPFC and Re-hippocampus connections.

To address this issue, the present study combined optogenetic activation of Re afferents with electrophysiological recordings of its postsynaptic targets in vitro and in vivo. These whole-cell patch-clamp recordings combined with pharmacological approaches provide detailed functional properties of Re-mPFC and Re-dorsal CA1 (dCA1) synapses and unmask a strong feedforward excitatory dynamic specific to mPFC. In vitro local field potential recordings in mPFC further confirmed the presence of this recurrent excitation of the mPFC network. Neuropixels probe single unit recordings in awake behaving animals revealed that activation of Re leads to both direct and delayed firing in mPFC, recapitulating observations made in vitro.

Altogether, these data show the functional synaptic connectivity, short-term plasticity profile, and neurotransmitter receptor expression level that underlie the function of the indirect pathway between dCA1 and mPFC through Re. They also show how the mPFC network uniquely amplifies Re output, which may be one of the mechanisms underlying modulation of memory retrieval.

Results

Re activation induces biphasic excitation in mPFC neurons.

Whole-cell patch-clamp recordings of mPFC neurons were obtained from acute brain slices from mice injected in Re with AAV1-CaMKIIa-ChR2-eYFP (Fig 1A). eYFP positive Re axons in mPFC showed expression in layer 1 and deep layers (Suppl. Fig 1A & Suppl. Fig 2), consistent with previous studies (3, 16). Activation of Re afferents could induce both action potential discharge and subthreshold EPSPs in mPFC neurons at their resting membrane potential (Fig 1B left). Interestingly, in addition to a reliable monosynaptic response seen at short latency (4.0+/-0.3 ms), a prominent second component, presumably reflecting polysynaptic excitatory input was observed in about half of the cases (8 of 18 cells, Fig 1B, bottom left). Blocking synaptic inhibition with picrotoxin, a $GABA_A$ receptor antagonist, led to late action potential firing (Fig 1B right) in 8/12 neurons (Fig 1C, left), which was not present in ACSF condition (Chi-square test, $p=2.4x10^{-4}$). The delayed firing consisted in a burst of 2 to 7 action potential, showing a latency ranging from 11 to 128 ms from light stimulation to first action potential peak (Fig 1C, right). This is much slower than the short-latency monosynaptic responses and suggests that recurrent network activity within mPFC is responsible for the late firing.

To examine the synaptic currents mediating these responses, we used whole-cell voltage-clamp recordings to obtain responses to blue light activation of Re inputs, which resulted in excitatory postsynaptic currents (EPSCs) at -70 mV and inhibitory postsynaptic currents (IPSCs) at +10 mV (Fig 1D). At -70 mV, the early EPSCs were time-locked to the light activation of Re axons and showed short latencies (4.4+/-0.3 ms) and sub millisecond jitter (0.36+/-0.05 ms) (Suppl. Fig1BC). In a subset of 6 cells, we blocked the light-evoked EPSCs with the sodium channel blocker, tetrodotoxin (TTX), and recovered them by bath application of the potassium channel blocker, 4-aminopyridine (4AP), confirming the monosynaptic nature of these synapses (17) (Suppl. Fig1DE). Holding the cell at the reversal potential for glutamatergic receptors (+10 mV in our recording condition, Fig 1D top) revealed a longer latency (IPSC: 7.8+/- 0.4 ms; EPSC: 4.0+/-0.3 ms) outward current that is sensitive to gabazine, consistent with a classical feedforward inhibitory circuit (Fig 1E, Wilcoxon signed-rank test, EPSC vs IPSC latency: $p=4.9x10^{-4}$). The excitation/inhibition (E/I) ratio at the Re-mPFC synapse was 2.3+/-0.9 (n=12) when measured in baseline conditions. The light-evoked EPSCs showed a NMDAR/AMPAR ratio of 0.21+/-0.03 (Suppl. Fig1G), with a significant contribution from GluN2B containing NMDARs (Suppl. Fig1H), and a short-term depression profile (Suppl. Fig1IJK) that is consistent with a high probability of release as shown in previous reports in rat (18).

Consistent with the polysynaptic responses observed in current-clamp recordings (Fig 1B), the EPSCs recorded at -70 mV were occasionally followed by late EPSCs (Fig 1D). Bath application of gabazine or

picrotoxin, $GABA_A$Rs blockers, resulted in either the new appearance or increase of this late EPSC (Synaptic charge, Baseline: -4+/-1 pC; Gabazine: -85+/-65 pC; Wilcoxon signed-rank test, p=0.03) without affecting the early component of the response (EPSC amplitude, Baseline: -85+/-34 pA; Gabazine: -68+/-31 pA; Paired Student's t test, p=0.07) (Fig 1E). Blockade of $GABA_A$Rs permitted stable recording of these late EPSCs, which showed longer latencies (18.9+/-3.3 ms) and a higher jitter (2.6+/-0.7 ms) than the early EPSCs (Fig 1FGH), which is consistent with a polysynaptic response (Latency: Wilcoxon signed-rank test, $p=1.9x10^{-9}$; Jitter: Wilcoxon signed-rank test, $p=1.5x10^{-5}$). The proportion of cells showing a late EPSCs in voltage-clamp mode increased in picrotoxin (Fig 1I) (Chi-square test, p=0.02). Most of the EPSCs showed a compound waveform that is intermediate between classical monophasic EPSCs and evoked responses with a well-separated late EPSC.

Bath application of APV, a NMDAR blocker, strongly reduced the amplitude, but did not eliminate, the late EPSCs (Fig 1JK). Subsequent bath application of DNQX completely abolished the late component (Friedman's test, $p=3.4x10^{-4}$, post hoc Wilcoxon signed-rank tests, BL vs APV: p= 0.008, APV vs DNQX: p=0.008, BL vs DNQX: p=0.008). By contrast, the early, presumed monosynaptic, component of the EPSC showed little to no reduction in its amplitude after bath application of APV and was fully blocked after subsequent application of DNQX (Friedman's test, $p=8.1x10^{-4}$, post hoc Wilcoxon signed-rank tests, BL vs APV: p= 0.11, APV vs DNQX: p=0.008, BL vs DNQX: p=0.008).

Altogether, these data show that activation of Re recruits a direct monosynaptic excitatory connection to mPFC neurons as well as both a classical feedforward inhibition and a novel feedforward excitation that to our knowledge has not previously been reported. The timing of the polysynaptic feedforward inhibition (11.9+/-1.9 ms, n=12) and polysynaptic feedforward excitation (18.9+/-3.2 ms, n=30) are similar, suggesting that the shunting effect of inhibitory synapses would reduce/occlude the late EPSCs. This is consistent with the finding that pharmacological blockade of $GABA_A$Rs unmasked the feedforward excitation in the mPFC network.

Re activation does not induce biphasic excitation in dCA1 pyramidal cells.

Axons expressing the ChR2-eYFP construct following Re injection were also found in the stratum lacunosum moleculare of the dCA1 region of hippocampus. Whole-cell patch-clamp recordings of dCA1 pyramidal neurons (Fig 2A) showed EPSCs at -70 mV and IPSCs at +10 mV upon light activation of Re axons. EPSCs were maintained in TTX/4AP, confirming the monosynaptic nature of these synapses. A subset of 3 neurons were recorded at +10 mV in TTX/4AP and showed that IPSCs were not recovered (Fig 2BC). Bath application of gabazine fully blocked IPSCs recorded at +10 mV (Fig 2D, top) without affecting the EPSCs (Fig 2D bottom and 2F) (Paired Student's t test for EPSC: p=0.052, Wilcoxon signed-rank tests for IPSC: p=0.002). The latencies of IPSCs were longer than EPSCs, consistent with a feedforward inhibitory circuit, and the E/I ratio was 0.5 +/- 0.1 (Fig 2E) (Wilcoxon signed-rank test, EPSC vs IPSC latency: $p=3.1x10^{-4}$). Trains of 10 blue light stimulations at 1 and 10 Hz revealed the short-term depression profile of the Re-dCA1 synapses (Fig 2GI). Interestingly, the 10 Hz train induced a rapidly developing, slowly decaying persistent current for both EPSC and IPSCs, which was absent during trains of stimulation at 1 Hz (Suppl. Fig1I-K). Altogether, these data show that Re axons form monosynaptic excitatory connections to dCA1 pyramidal neurons and recruit feedforward inhibition, likely through activation of neurogliaform cells located in the stratum lacunosum moleculare (19). Delayed EPSCs, as seen in mPFC neurons upon activation of Re afferents, were not observed in dCA1 pyramidal cells, even in the presence of $GABA_A$R blockers. This suggests that Re inputs are specifically enhanced by mPFC circuitry, pointing towards a specialized feature of local mPFC networks that promotes recurrent excitation.

$GABA_A$R blockade reveals the delayed activation of mPFC local network upon Re activation.

We next examined the laminar structure of Re activation across mPFC cortical columns in an effort to get insights into the anatomical origins of the observed biphasic excitation. Slices collected from C57BL6/J were recorded using a 16-shank electrode array spanning across cortical layers (Fig 3A). Blue light activation of Re afferents resulted in local field potentials in the mPFC from which were derived as current

source density (CSD) (Fig 3B). Pairs of sinks and sources were observed following optogenetic stimulation of Re afferents, attributed to cations flowing from the extracellular space into the cells during synaptic excitation, and flowing back out of cells at a distance, respectively. Similarly, during synaptic inhibition, current sources are seen at locations of inhibitory synapses where chloride ions flow into cells, and sinks at other sites where current flows back out of cells. Sources and sinks were prominent within the first 10 ms after the light onset in layer 2 and 3 (L2/3) and to a lesser extent in layer 5 (L5) (Fig 3BD). Bath application of gabazine had little to no effect on these early sinks and sources (Wilcoxon signed-rank tests, L2/3 early source p=0.03, L2/3 early sink p=0.09, L5 early source p=0.06, L5 early sink p=0.25). However, the blockade of $GABA_A$Rs revealed Re-induced delayed sinks and sources throughout the cortical column that lasted for hundreds of ms (Wilcoxon signed-rank tests, L2/3 late source $p=6.2x10^{-5}$, L2/3 late sink $p=6.1x10^{-5}$, L5 late source $p=6.1x10^{-5}$, L5 late sink $p=6.1x10^{-5}$) (Fig 3CDE). This delayed network activity in the mPFC is reminiscent of the late EPSCs and delayed firing observed in single cell recordings (Fig 1H). Re-dependent optogenetic excitation of mPFC network with delay was visible in 1/15 slices in ACSF and further amplified in gabazine (Suppl. Fig 4). Electrical stimulation of the layer 1 of mPFC yielded similar results, with bath application of gabazine revealing delayed sinks and sources across the cortical column (Suppl. Fig 5) (Wilcoxon signed-rank tests, L2/3 late source p=0.01, L2/3 late sink p=0.002, L5 late source p=0.002, L5 late sink p=0.006). These results demonstrate that mPFC amplification of Re inputs involves recurrent activity within the cortical column which can be revealed through blockade of concurrent feedforward inhibition. The observed similarity in delayed mPFC activation following both electrical stimulation of layer 1 in the presence of a GABAAR blocker and optogenetic stimulation of Re axons strongly implies that these specialized characteristics of the mPFC network, amplifying Re inputs, may extend to other higher-order thalamic inputs targeting mPFC layer 1, such as those from the mediodorsal and ventromedial thalamus.

Activation of Re leads to biphasic excitation of mPFC units *in vivo*.

The single cell and transcolumnar recordings in slices revealed that Re can induce feedforward excitation in mPFC. This feedforward excitation was particularly pronounced upon blocking $GABA_A$R. To address whether the cortical amplification of thalamic input in mPFC is present in vivo, we recorded local field potential and single units in the mPFC of four C57BL6/J mice using Neuropixels probes, with combined optogenetic activation of Re (Fig 4A). Probes were acutely inserted at a 45-degree angle and traversed mPFC in both hemispheres (Fig 4B). Probe tracks were reconstructed in 3D using the SHARP-Track Matlab suite (Fig 4C). Optogenetic activation of Re induced a succession of deflections in the local field potential measured from electrodes located in the mPFC (Fig 4DE). The CSD derived from these local field potentials confirmed that the major source of synaptic response was in the L2/3 of mPFC (Suppl. Fig 6). Delayed deflections in the local field potential, reminiscent of the ones observed in slices (Fig 3), were also observed in the deep layer of mPFC.

Recorded units were ordered according to their position along the probe (Fig 4F). Optogenetic activation of Re induced variable patterns of changes in the firing rate of mPFC units. Responding units often showed a mixed pattern of early increase in firing followed by a decrease in firing and/or a delayed increase in firing (Fig 4G). Overall, 48 units out of 135 responded to activation of Re (Fig 4H). 46 units showed an early increase in firing rate starting 7+/-1 ms after the light onset. 22 units showed a decrease in firing rate that started 36+/-3 ms after the light onset. 22 units showed a delayed increase in firing rate that started 146+/-7 ms after the light onset and lasted for tens of ms (Fig 4I) (Kruskal–Wallis H test $p=2.2x10^{-16}$, Wilcoxon rank sum tests, Early vs Reduction $p=3.7x10^{-11}$, Early vs Delay $p=2.1x10^{-11}$, Reduction vs Delay $p=7.8x10^{-8}$). This delayed increase in firing rate upon activation of Re afferents in awake behaving mice suggests that mPFC amplification of thalamic input occurs in vivo during behavior.

Taken together, the results of these in vivo recordings show that, in addition to triggering direct excitation and feedforward inhibition, Re inputs induce recurrent network activity as measured by delayed firing of mPFC units.

Discussion

The mPFC and hippocampus are well-known for their roles in memory formation and retrieval (1, 20, 21). However, how the interactions between these two structures underlies these functions is not fully understood. The direct pathway between vCA1 and mPFC is involved in social memory and emotional regulation (22). However, dCA1, a region critical for spatial and contextual memory (23), show little to no direct projections to mPFC (24, 25). Similarly, mPFC show little to no direct projections to hippocampus (20). The mPFC plays a role in directing the retrieval of contextual memories even in the absence of a direct pathway to the hippocampus (20), revealing the importance of indirect pathways, notably through the Re in the midline thalamus, for spatial and emotional memory processing.

The Re sends and receives inputs to and from mPFC and hippocampus and can modulate the activity of both structures (3). Our data showed that Re sends monosynaptic excitatory projections to both structures. Re-mPFC and Re-dCA1 synapses on pyramidal cells both showed a strong short-term depression, supporting the idea that they are high release probability synapses (26). This short-term depression profile at 10 Hz is consistent with a previous report using similar whole-cell patch-clamp and optogenetic approach in rats (18). Optogenetic activation of Re-mPFC and Re-dCA1 synapses also resulted in strong feedforward inhibition of pyramidal cells, consistent with previous reports (19, 27, 28). Interestingly, Re activation produced a strong polysynaptic feedforward excitation of mPFC pyramidal cells, which was particularly evident upon pharmacological blockade of the feedforward inhibition. Activation of Re-dCA1 synapses did not result in a similar feedforward excitation, suggesting a specialized feature of the Re-mPFC subsystem. Consistent with the observations of delayed EPSC and delayed firing in single cell recordings and transcolumnar CSD recording in slices, single unit *in vivo* showed a similar delayed firing of mPFC network upon activation of Re inputs. The latencies between light stimulation of Re or its axons and the onset of delayed excitatory current/delayed firing varies between recording methods, likely reflecting differences in experimental conditions and network state. Regardless of this discrepancy, all three approaches revealed a consistent delayed excitation in mPFC upon activation of Re.

These results suggest that the indirect pathway between hippocampus and mPFC via the Re can recruit recurrent and long-lasting activity in mPFC. This activity could act as a gating mechanisms or coincidence detector for direct input from vCA1 to mPFC, contributing to hippocampal-mPFC synchrony for contextual cue encoding (29). Our data also suggests that the feedback from mPFC to dCA1 via Re, relevant for biased memory retrieval, has an acute effect on hippocampal function, with a rapid recruitment of feedforward inhibition (Fig. 2).

The biphasic excitation of the mPFC upon activation of Re afferents is likely mediated by direct excitation and polysynaptic feedforward excitation. Cortical columns contain major interactions between excitatory cells across layers, which is preserved across the neocortex and plays a major role in the integrative function of the cortex (30). Local connectivity between L2/3 and L5 of mPFC is a likely candidate to explain the biphasic excitation of mPFC upon activation of Re. Both L2/3 and L5 pyramidal cells receive direct synaptic inputs from Re (3), which can lead to action potential discharge from neurons in both layers. Recurrent connectivity within and across layers in mPFC (31, 32) could then lead to a second, delayed excitation. Interestingly, higher order thalamic nuclei have been shown to facilitate generation of dendritic plateau potentials in cortical pyramidal neurons (33). Re axons in L1 likely target apical dendrites of L2/3 and L5 pyramidal cells. Glutamate release on these apical dendrites could generate dendritic plateau potentials, putting the neuron in an “activated state”. This activated state has been shown to operate as a time window on the order of hundreds of ms during which cortical neurons are particularly excitable and more likely to respond to afferent inputs with spike discharge (34). This phenomenon could create a temporal window during which other inputs to mPFC could be amplified, notably the direct pathway from vCA1 that is important for contextual cues encoding. Delayed firing of mPFC neurons is unlikely to be explained by rebound firing following an inhibitory input. Indeed, the delayed excitation/bursting recorded in mPFC neurons is amplified upon long-lasting $GABA_A$Rs blocking (Fig. 1&3), suggesting that the delayed

excitation is due to the recurrent excitatory network within mPFC rather than rebound firing following feedforward inhibition.

The small size and position of Re makes it hard to target specifically with viral injection. Small spill out of viral vectors into neighboring midline and intralaminar thalamic nuclei that sends projections to mPFC can lead to expression of ChR2 in their axons (35). Differences in axonal propagation of the signal from distinct thalamic nuclei could explain short delays in synaptic responses. However, optogenetic stimulations in slices were done at the release site, reducing the impact of inter-region axonal propagation delays. Similarly, polysynaptic connections from Re to other cortical/subcortical structures, then to mPFC could explain the delayed excitation. While this possibility cannot be excluded during the *in vivo* recordings (Fig. 4) where the brain is fully intact, this is unlikely in ex vivo slice recording as only local axons are intact (Fig. 1&3). Could the biphasic excitation be due to an unexpected effect of ChR2 on the neurotransmitter release of Re axons? Electrical stimulation of L1 produced a similar biphasic excitation in the mPFC columns (Suppl. Fig. 5), excluding the idea of ChR2 inducing an unexpected biphasic activation of Re axons. This also suggests that activation of other structures projecting to mPFC through L1, such as the mediodorsal thalamus, would result in a similar biphasic excitation. Note that this biphasic excitation was *not* observed in dCA1 pyramidal cells upon activation of Re axons, further suggesting that the mechanism underlying delayed excitation resides in the local network connectivity rather than the Re axons themselves.

The mPFC plays a crucial role in integrating information from its numerous cortical and subcortical afferents and to converge updated information to its targets (36). The biphasic excitation of mPFC neurons we observed, especially the delayed bursting in single cell recordings, is significant as it can amplify the transmission of information to its targets. The propensity of the mPFC for biphasic excitation may act as an integrator where a delayed discharge occurs upon synchronized inputs to mPFC. Overall our work suggests that mPFC, but not dCA1, contains the necessary local circuitry for sustaining Re coordinated information transferred between these memory and executive function related brain regions.

This study provides robust physiological characterization of the synaptic properties of the Re-mPFC and Re-dCA1 circuits and reveals an unprecedented recruitment of feedforward excitation of the mPFC by a thalamic input. This biphasic excitation may underlie the role of mPFC in integrating information, maintain it in working memory, and in providing a strong overriding output to its postsynaptic targets upon synchronized input to mPFC.

Materials and Methods

Experimental model and subject details

All experimental procedures were performed in accordance with the guidelines of the Institutional Animal Care and Use Committees of Stanford University. Young adult (4 to 8 weeks old) C57BL/6J mice (M. musculus, Jackson Laboratory, RRID: IMSR_JAX:000664) of either sex were housed prior to experiment in a temperature and humidity-controlled animal house. They were maintained in a 12 h/12 h light-dark cycle and could access food and water ad libitum.

Anterograde tracing

Iontophoretic injection of *Phaseolus Vulgaris-leucoagglutinin* (PHAL-L, Vector Laboratories, Cat. No. L-1110) has been described in detail in (37). Briefly, mice were anesthetized with isoflurane (5% induction, 2% maintenance) and received Carprofen (5 mg/kg i.p.). Craniotomies were performed above the injection sites (in mm from bregma, AP, ML, DV: mPFC +2, $\pm$0.5, -2; dCA1 -3.8, $\pm$3.3, -2.5, Re 30° diagonal injection -0.75, -2.31, -4.62). PHAL-L was electroporated with a 5-mA positive current, 7 s on/off loop for 15 min, applied with a home-made current isolator and a Master-8 (Master-8 Pulse Stimulator, A.M.P.I., Jerusalem, Israel). A lethal dose of pentobarbital was injected i.p. prior to intracardial injection of paraformaldehyde 4% (~2.5 ml/min). Brains were post-fixed overnight at 4°C in paraformaldehyde 4%, washed 3 times in phosphate buffer (PB) 0.1 M and fixed in a sucrose solution (30% sucrose) overnight at room temperature.

100 µm-thick brain slices were obtained with a vibratome (Microtome Leica VT1000 S; speed: 0.25 – 0.5 mm s-1 and knife sectioning frequency: 65 Hz) or a freezing microtome (Microm) and transferred to individual wells in plates filled with 0.1 M PB for immunohistochemistry. After washing the brain slices with PB 0.1 M, slices were transferred into a blocking solution (PB 0.1M, Triton 0.3%, NGS 2%) for 30 min, a first antibody solution (PB 0.1M, Triton 0.3%, NGS 2%, Rabbit α-Phal-L 1:8000 (Vector Laboratories, AS-2300, RRID: AB_2313686), Mouse α-PV 1:4000 (Swant, PV235, RRID: AB_10000343) for 48 h at 4°C, washed 3 times in PB 0.1 M, a secondary antibody solution (PB 0.1M, Triton 0.3%, NGS 2%, goat anti-rabbit Cyanine Cy3™ (Jackson Immunoresearch, 111-165-003, RRID: AB_2338000), goat anti-mouse Cy5™ (Jackson Immunoresearch, 115-175-146, RRID: AB_2338713) for 24 h at 4°C, washed 3 times in PB 0.1 M and mounted on slides. Brain slices were imaged using a fluorescent stereomicroscope (Nikon SMZ 25). The micrographs were processed using NIS-Elements 4.5 (Nikon), Adobe Photoshop CS5 (Adobe Creative Cloud) and Adobe Illustrator (Adobe Creative Cloud).

Viral injections

The procedure for viral injection has been described in detail in (37). Briefly, young adult mice were anesthetized with Ketamine-Xylazine (83 and 3.5 mg/kg, respectively) or isoflurane (5% induction, 2% maintenance) and received Carprofen 5 mg/kg i.p. Mice received a single injection in the Re (in mm from bregma, AP -0.75, ML 0, DV -4). A volume of 0.2 to 0.5 µl of virus encoding the ChR2 (AAV1-CaMKIIa-ChR2(H134R)_eYFP-WPRE-HGH, 10^{12} GC, 100 nl/min, Penn Vector Core, Addgene 26969P) was delivered at the injection site.

In vitro patch-clamp recording

Solutions for slice preparation and recording

Mouse brains were extracted, sliced with a vibratome (Leica VT1200S) and recorded using standard procedures (37). In brief, 300 µm-thick coronal brain slices were obtained in an ice-cold oxygenated slicing solution containing in mM: 66 NaCl, 2.5 KCl, 1.25 NaH_2PO_4, 26 $NaHCO_3$, 105 D(+)-sucrose, 27 D(+)-glucose, 1.7 L(+)-ascorbic acid, 0.5 $CaCl_2$ and 7 $MgCl_2$. Slices were then kept in a recovery chamber at 35°C for 30 min then at room temperature for at least 30 more minutes before recording. The chamber was filled with a recovery solution containing, in mM: 131 NaCl, 2.5 KCl, 1.25 NaH_2PO_4, 26 $NaHCO_3$, 20 D(+)-glucose, 1.7 L(+)-ascorbic acid, 2 $CaCl_2$, 1.2 $MgCl_2$, 3 myo-inositol, 2 pyruvate. The artificial cerebrospinal fluid (ACSF) used for recording contained, in mM: 131 NaCl, 2.5 KCl, 1.25 NaH_2PO_4, 26 $NaHCO_3$, 20 D(+)-glucose, 1.7 L(+)-ascorbic acid, 2 $CaCl_2$, 1.2 $MgCl_2$, 0.01 glycine and was supplemented with 0.1 picrotoxin (Abcam, ab120315) when appropriate. Cesium-based intracellular solution contained in mM: 127 CsGluconate, 10 HEPES, 2 CsBAPTA, 6 $MgCl_2$, 10 phosphocreatine, 2 Mg-ATP, 0.4 Na-GTP, 2 QX314-Cl (Tocris, 2313), pH 7.3, 290–305 mOsm. The potassium-based intracellular solution contained in mM: 144 KGluconate, 10 HEPES, 3 $MgCl_2$, 0.5 EGTA, pH 7.3, 290–305 mOsm. Series and input resistances were monitored throughout recordings by brief voltage and current pulses, for voltage- and current-clamp recordings, respectively. Data were excluded for Rs and Ri changes above 20%.

Properties of excitatory synapses

ChR2-expressing Re afferents to dCA1 and mPFC neurons were activated using blue LEDs stimulation (Cairn Res, Faversham, UK, 455 nm, duration: 1 ms, maximal light intensity 3.5 mW, 0.16 mW/mm^2; Thorlabs M450LP2, 450 nm, duration 1 ms, maximal light intensity 13 mW, 19 mW/cm^2) or blue lasers (Laserglow Technologies, 473 nm, duration 1 ms, maximal light intensity 8 mW, 10.8 mW/cm^2).

The short-term plasticity profile of the Re-dCA1 and Re-mPFC synapses was measured in voltage-clamp mode at -70 mV, using 10 light stimulations at 1 Hz and 10 Hz, one train of stimulation every 20 s.

To confirm the monosynaptic nature of the Re-dCA1 and Re-mPFC connections, single light pulses were used to activate Re afferents once every 10 s. Action potential-dependent light evoked EPSCs in dCA1/mPFC were blocked with tetrodotoxin (TTX, Latoxan L8503) 0.25 µM. Action potential-independent

light evoked responses were then recorded subsequent to bath application of 4-aminopyridine (4AP, Abcam, ab120122) 100 µM.

The subunit content of the Re-mPFC synapses was assessed using successive bath application of ionotropic glutamate receptor blockers. The AMPA receptor mediated currents were recorded at -70 mV for at least 2 min of stable baseline and then blocked with 6,7-dinitroquinoxaline-2,3(1H,4H)-dione (DNQX, Abcam, ab120169) 40 µM. The membrane potential was brought at +40 mV to release the magnesium block and show NMDA receptor mediated currents. After a baseline recording, the NMDA receptors were partially or completely blocked using NVP-AAM077 (NVP, Novartis Pharma) 0.05 µM (a competitive antagonist with higher selectivity for GluN2A containing NMDA receptors (38)), CP-101.606 (CP, Pfizer Pharmaceuticals) 10 µM (GluN2B specific blocker (39)), (2S*,3R*)-1-(Phenanthren-2-carbonyl)piperazine-2,3-dicarboxylic acid (PPDA, Tocris Bioscience, 2530) 0.5 µM (NMDA receptor antagonist that preferentially binds to GluN2C/GluN2D (40)) or DL-2-Amino-5-phosphonovaleric acid (APV, Sigma, A5282) 100 µM (broad spectrum NMDA receptor blocker).

Feedforward inhibition

A subset of recordings was done without picrotoxin to investigate whether Re neurons recruit feedforward inhibition onto dCA1 and mPFC cells. A single light stimulation was used to activate ChR2-expressing Re afferents. dCA1 and mPFC neurons were recorded in voltage-clamp at -70 mV then at +10 mV to show EPSC and IPSC respectively. The IPSCs were then blocked with Gabazine (Abcam, ab120042) 10 µM in a subset of experiments.

Cellular properties and synaptic depolarization

Passive cellular properties were recorded in voltage clamp at resting levels of -60 to -70 mV, using a 500 ms-long hyperpolarizing step of 10 mV or in current-clamp from the resting membrane potential. Action potential properties were measured at the rheobase in current-clamp mode, with a membrane potential held at ~ -60 mV and using 500 ms-long depolarizing current steps of increasing amplitude. The effect of Re afferent activation on the membrane potential of dCA1 and mPFC neurons was measured in current-clamp mode, with a holding membrane potential around -60 mV. Re afferents were activated by a train of 10 light pulses at 1 and 10 Hz, one train every 20 s.

In vitro local field potential recordings

Extracellular recordings were conducted using 400 µm-thick coronal brain slices containing the mPFC obtained from mice expressing the ChR2-eYFP in Re after viral injection. The experimental setup involved placing the slices in a humidified, oxygenated interface chamber at a constant temperature of 34°C and perfusing them with oxygenated ACSF at a rate of 2 ml/min. Local field potential (LFP) were measured with a linear silicon multichannel probe (NeuroNexus Technologies) with 16 channels and 100 µm inter-electrode spacing, which was placed perpendicular to the laminar plane across all mPFC layers.

The multichannel probe was connected to a pre-amplifier (PZ5-32, Tucker-Davis Technologies (TDT)), and data were stored using a RZ5D processor multichannel workstation (TDT). Recording sessions were designed with the Real-time Processor Visual Design Studio (RPvdsEx) tool and custom Python code. LFP data were acquired at 25 kHz frequency and band-passed between 0.1 and 500 Hz.

Optogenetic stimulations were delivered using a blue laser (Laserglow Technologies, 473 nm, duration 5 ms, maximal light intensity 15 mW, 20 mW/cm^2). The blue light stimulation encompassed a circular area of about 1 mm in diameter spanning across all cortical layer in mPFC. Electrical stimulations were delivered by a bipolar tungsten microelectrode (with each wire having a resistance of 50-100 kΩ, duration 0.1 ms, intensity 500 µA) that was precisely positioned in layer 1 of the mPFC. Both stimulations were done as a single pulse, once every 20 s. Each successive recording conditions (baseline, gabazine, DNQX/AP5, TTX) were recorded for 5 min but only the last 2 min were used for analysis, leaving enough time to reach a steady state in the different drug conditions.

To accurately characterize the location, direction, and magnitude of currents associated with the synchronous network activity, we derived the current-source density (CSD) from the raw LFP signals (41). We assumed a uniform conductivity of 0.3 S/m across all layers (42). The CSD was computed in the mPFC by performing second order algebraic differentiation of the LFP signals recorded at adjacent electrodes in the linear probe. The ion flow in and out of the extracellular space created sinks and sources of current in the CSD, which can then be attributed to specific cortical layers. Successive pharmacological blockade of postsynaptic receptors and action potential generation allowed to disentangle the origins of the recorded sinks and sources in mPFC.

Acute *in vivo* Neuropixels recordings

Mouse preparation

Four female C57BL6/J mice (P110-P120) were injected with AAV1-CaMKIIa-ChR2(H134R)_eYFP-WPRE-HGH as described above. An optical fiber (200 µm core, 0.22-NA, 2.5 mm-diameter ceramic ferrule, Thorlabs) was implanted 200 µm above the viral injection site. A miniature self-tapping screw (stainless steel, J.I Morris Company FF00CE125) connected to a pin (Mill-Max 853-93-100-10-001000) was inserted into the occipital bone over the cerebellum as a reference. A gold pin (1.27 mm, Mill-Max Manufacturing Corp.) was implanted in contact with the surface of primary somatosensory cortex and served as an EEG electrode to validate that no pathological activity, e.g., seizures, were induced. A custom metal head bar (eMachineShop) was placed and stabilized using dental cement (Metabond). After surgery, animals recovered for one week before being trained for handling and head restriction on a cylindrical treadmill. Recordings were performed after habituation over one to two weeks of training.

On recording day 1, a 1 mm craniotomy was performed with a 0.5 mm burr dental drill (Fine Science Tools) over the right motor cortex (AP: 1.5 to 2.5 mm, ML: 1 to 2 mm) and sealed with a removable silicone sealant (Kwik-Cast, World Precision Instrument). Mice were left to recover for at least 4h in their home cage before recording. Mice were head fixed on the cylindrical treadmill and an optic fiber was connected via the ceramic ferrule/optic fiber previously mounted on the mouse. The other end of the optic fiber was connected to a laser (OEM Laser Systems, 473 nm, duration 5ms, maximal light intensity 3.2 mW, 4.5 mW/cm^2), while the EEG gold pin and reference screw were connected to an Intan headstage (RHD 2132) and OpenEphys acquisition board. The silicone sealant was removed from the craniotomy and a Neuropixels 1.0 probe previously dipped in red dye (Vybrant DiD cell labeling solution, ThermoFisher Scientific) was connected via cable to the PXIe data acquisition system (National Instrument NI-PXIe-1071) then positioned above the cortex.

Recording

The Neuropixels probe was slowly inserted over ~5 minutes using a Sutter MP285 micromanipulator system at a 45-degree angle into the brain of the awake, head-fixed mouse, followed by about an hour of recording. This electrode array recorded 384 channels, spanning a 3.8mm of the brain across motor cortex and mPFC, traversing the midline. The probe was allowed to settle for ~20 min before starting the recording. Recording sessions consisted of 5 min of baseline followed by 5 min of optogenetic stimulation at either 1 or 10 Hz. Trains of stimulation were given once every 20 s and consisted of 2 (at 1 Hz) or 11 (at 10 Hz) 5-ms long pulses. Data were acquire using OpenEphys software (https://open-ephys.org/) at 30 kHz.

Analysis

The data were spike-sorted automatically by Kilosort2.5 (https://github.com/MouseLand/Kilosort) followed by manual curating using Phy2 (https://github.com/cortex-lab/phy). Single unit clusters with inter-spike-interval violations > 0.05% (calculated as the ratio of the spikes within the refractory period ±1.5 ms to the total number of spikes) were removed. Single unit clusters that were not stable throughout the 10 min recording sessions were excluded from analysis. Custom Matlab code (www.mathworks.com) were used to plot peri-stimulus raster plots and peri-event time histogram (in 5 ms bin) from 50 ms before to 250 ms

after laser stimulation. Z-scores were calculated using the 50 ms prior to laser stimulation as a baseline. Changes in firing rate were classified as “early increase” when occurring between 0 and 15 ms following laser stimulation, delayed increase when occurring > 20 ms after laser stimulation, or reduction in firing.

Histology and probe localization

Mice were sacrificed with an intraperitoneal injection of Fatal+ (Pentobarbital, Vortech Pharmaceutical). Cardiac perfusion was performed with 4% paraformaldehyde in PBS. The brains were post-fixed overnight in 4% paraformaldehyde, rinsed in PBS and sliced using a vibratome (Leica VT1000S). The 100 µm-thick brain slices containing the recording site in mPFC and the viral injection site in the Re were mounted in DAPI-Fluoromount-G (Southern Biotech 0100-20). Epifluorescent micrographs for DAPI, ChR2-eYFP and probe track were obtained using a Zeiss microscope (Zeiss Axio Imager M2). SHARP-track (Allen CCF tools) was used to reconstruct the Neuropixels probe track in 3D and to localize recording sites. SHARP-track allows the 3D reconstruction of the Neuropixels probe within the Allen Mouse Brain Common Coordinate Framework based on the histology and physiological landmarks. Each channel was then attributed to its corresponding brain regions in motor cortex or mPFC. A few channels with units were found in the dorsal peduncular cortex or the olfactory bulbs and were discarded from analysis.

Quantification and statistical analysis

The R programming software (3.6.1, The R Foundation for Statistical Computing, 2019] and Prism 6 (GraphPad Software Inc) were used for statistical analysis. The Shapiro-Wilk normality test was used to assess the normality of the dataset distribution. Accordingly, comparison of two datasets were done using Student’s *t* test and paired Student’s *t* test for non-repeated and repeated measures, respectively. Their non-parametric equivalent, Wilcoxon rank sum test and Wilcoxon signed rank test, were used when at least one of the datasets was not normally distributed. Comparisons of more than 2 datasets were done using ANOVA tests or their non-parametric equivalents when appropriate. The Šidák correction was used to adjust the α threshold for significance when the analysis required multiple comparisons. Significant exact p values are indicated in the main text. On figures, significance levels are abbreviated as * ($p < 0.05$), ** ($p < 0.01$) and *** ($p < 0.001$). Detailed statistics can be found in Table 1.

Acknowledgments

We thank Prof. Anita Lüthi for providing lab space, equipment, and overall support during the initial phase of the project. We thank all lab members for constructive input for the manuscript and discussions during the project. We thank Nicole Agranonik, Cameron Glick and Katlin Villar for their help in managing mouse lines, laboratory equipment and supplies.

Funding sources

This work was supported by the Swiss National Science Foundation (P2LAP3-199556); Wu Tsai Neuroscience Institute, and NINDS (NS34774).

References

1. A. R. Preston, H. Eichenbaum, Interplay of Hippocampus and Prefrontal Cortex in Memory. *Curr. Biol.* **23**, R764–R773 (2013).

2. B. P. Godsil, J. P. Kiss, M. Spedding, T. M. Jay, The hippocampal–prefrontal pathway: The weak link in psychiatric disorders? *Eur. Neuropsychopharmacol.* **23**, 1165–1181 (2013).

3. M. J. Dolleman-van Der Weel, *et al.*, The nucleus reuniens of the thalamus sits at the nexus of a hippocampus and medial prefrontal cortex circuit enabling memory and behavior. *Learn. Mem.* **26**, 191–205 (2019).

4. V. Kafetzopoulos, *et al.*, The nucleus reuniens: a key node in the neurocircuitry of stress and depression. *Mol. Psychiatry* **23**, 579–586 (2018).

5. A. Roy, F. P. Svensson, A. Mazeh, B. Kocsis, Prefrontal-hippocampal coupling by theta rhythm and by 2–5 Hz oscillation in the delta band: The role of the nucleus reuniens of the thalamus. *Brain Struct. Funct.* **222**, 2819–2830 (2017).

6. M. Ferraris, *et al.*, The Nucleus Reuniens Controls Long-Range Hippocampo–Prefrontal Gamma Synchronization during Slow Oscillations. *J. Neurosci.* **38**, 3026–3038 (2018).

7. M. Jayachandran, *et al.*, “Reuniens transiently synchronizes memory networks at beta frequencies” (Neuroscience, 2022).

8. J.-C. Cassel, *et al.*, The reuniens and rhomboid nuclei of the thalamus: A crossroads for cognition-relevant information processing? *Neurosci. Biobehav. Rev.* **126**, 338–360 (2021).

9. D. Jung, Y. Huh, J. Cho, The Ventral Midline Thalamus Mediates Hippocampal Spatial Information Processes upon Spatial Cue Changes. *J. Neurosci.* **39**, 2276–2290 (2019).

10. G. R. I. Barker, E. C. Warburton, A Critical Role for the Nucleus Reuniens in Long-Term, But Not Short-Term Associative Recognition Memory Formation. *J. Neurosci.* **38**, 3208–3217 (2018).

11. J. A. Prasad, A. R. Abela, Y. Chudasama, Midline thalamic reuniens lesions improve executive behaviors. *Neuroscience* **345**, 77–88 (2017).

12. S. B. Linley, M. M. Gallo, R. P. Vertes, Lesions of the ventral midline thalamus produce deficits in reversal learning and attention on an odor texture set shifting task. *Brain Res.* **1649**, 110–122 (2016).

13. F. Troyner, M. A. Bicca, L. J. Bertoglio, Nucleus reuniens of the thalamus controls fear memory intensity, specificity and long-term maintenance during consolidation. *Hippocampus* **28**, 602–616 (2018).

14. T. D. Viena, S. B. Linley, R. P. Vertes, Inactivation of nucleus reuniens impairs spatial working memory and behavioral flexibility in the rat. *Hippocampus* **28**, 297–311 (2018).

15. D. J.-N. Maisson, Z. M. Gemzik, A. L. Griffin, Optogenetic suppression of the nucleus reuniens selectively impairs encoding during spatial working memory. *Neurobiol. Learn. Mem.* **155**, 78–85 (2018).

16. R. P. Vertes, S. B. Linley, W. B. Hoover, LIMBIC CIRCUITRY OF THE MIDLINE THALAMUS. *Neurosci. Biobehav. Rev.* **54**, 89–107 (2015).

17. L. Petreanu, T. Mao, S. Sternson, K. Svoboda, The subcellular organization of neocortical excitatory connections. *Nature* **457**, 1142–1145 (2009).

18. P. J. Banks, E. C. Warburton, Z. I. Bashir, Plasticity in Prefrontal Cortex Induced by Coordinated Synaptic Transmission Arising from Reuniens/Rhomboid Nuclei and Hippocampus. *Cereb. Cortex Commun.* **2**, tgab029 (2021).

19. P. Goswamee, E. Leggett, A. R. McQuiston, Nucleus Reuniens Afferents in Hippocampus Modulate CA1 Network Function via Monosynaptic Excitation and Polysynaptic Inhibition. *Front. Cell. Neurosci.* **15**, 660897 (2021).

20. J. Jin, S. Maren, Prefrontal-Hippocampal Interactions in Memory and Emotion. *Front. Syst. Neurosci.* **9** (2015).

21. D. R. Euston, A. J. Gruber, B. L. McNaughton, The Role of Medial Prefrontal Cortex in Memory and Decision Making. *Neuron* **76**, 1057–1070 (2012).

22. M. L. Phillips, H. A. Robinson, L. Pozzo-Miller, Ventral hippocampal projections to the medial prefrontal cortex regulate social memory. *eLife* **8**, e44182.

23. S. Daumas, H. Halley, B. Francés, J.-M. Lassalle, Encoding, consolidation, and retrieval of contextual memory: Differential involvement of dorsal CA3 and CA1 hippocampal subregions. *Learn. Mem.* **12**, 375–382 (2005).

24. T. M. Jay, M. P. Witter, Distribution of hippocampal CA1 and subicular efferents in the prefrontal cortex of the rat studied by means of anterograde transport of Phaseolus vulgaris-leucoagglutinin. *J. Comp. Neurol.* **313**, 574–586 (1991).

25. M. S. Fanselow, H.-W. Dong, Are the Dorsal and Ventral Hippocampus Functionally Distinct Structures? *Neuron* **65**, 7–19 (2010).

26. S. M. Sherman, “Functioning of Circuits Connecting Thalamus and Cortex” in *Comprehensive Physiology*, (John Wiley & Sons, Ltd, 2017), pp. 713–739.

27. A. Kamalova, *et al.*, CCK+ interneurons contribute to thalamus-evoked feed-forward inhibition in prelimbic prefrontal cortex. *J. Neurosci.* (2024). https://doi.org/10.1523/JNEUROSCI.0957-23.2024.

28. S. J. Cruikshank, *et al.*, Thalamic Control of Layer 1 Circuits in Prefrontal Cortex. *J. Neurosci.* **32**, 17813–17823 (2012).

29. H. Eichenbaum, Prefrontal–hippocampal interactions in episodic memory. *Nat. Rev. Neurosci.* **18**, 547–558 (2017).

30. R. J. Douglas, K. A. C. Martin, Neuronal Circuits of the Neocortex. *Annu. Rev. Neurosci.* **27**, 419–451 (2004).

31. K. D. Harris, G. M. G. Shepherd, The neocortical circuit: themes and variations. *Nat. Neurosci.* **18**, 170–181 (2015).

32. Y. Printz, *et al.*, Determinants of functional synaptic connectivity among amygdala-projecting prefrontal cortical neurons in male mice. *Nat. Commun.* **14**, 1667 (2023).

33. S. Pagès, *et al.*, An increase in dendritic plateau potentials is associated with experience-dependent cortical map reorganization. *Proc. Natl. Acad. Sci.* **118**, e2024920118 (2021).

34. P. P. Gao, *et al.*, Local glutamate-mediated dendritic plateau potentials change the state of the cortical pyramidal neuron. *J. Neurophysiol.* **125**, 23–42 (2021).

35. W. B. Hoover, R. P. Vertes, Anatomical analysis of afferent projections to the medial prefrontal cortex in the rat. *Brain Struct. Funct.* **212**, 149–179 (2007).

36. E. K. Miller, J. D. Cohen, An integrative theory of prefrontal cortex function. *Annu. Rev. Neurosci.* **24**, 167–202 (2001).

37. G. Vantomme, *et al.*, A Thalamic Reticular Circuit for Head Direction Cell Tuning and Spatial Navigation. *Cell Rep.* **31**, 107747 (2020).

38. P. A. Frizelle, P. E. Chen, D. J. A. Wyllie, Equilibrium Constants for (R)-[(S)-1-(4-Bromo-phenyl)-ethylamino]-(2,3-dioxo-1,2,3,4-tetrahydroquinoxalin-5-yl)-methyl]-phosphonic Acid (NVP-AAM077) Acting at Recombinant NR1/NR2A and NR1/NR2B N-Methyl-d-aspartate Receptors: Implications for Studies of Synaptic Transmission. *Mol. Pharmacol.* **70**, 1022–1032 (2006).

39. F. S. Menniti, *et al.*, CP-101,606: An NR2B-Selective NMDA Receptor Antagonist. *CNS Drug Rev.* **4**, 307–322 (1998).

40. B. Feng, *et al.*, Structure–activity analysis of a novel NR2C/NR2D-preferring NMDA receptor antagonist: 1-(phenanthrene-2-carbonyl) piperazine-2,3-dicarboxylic acid. *Br. J. Pharmacol.* **141**, 508–516 (2004).

41. J. A. Freeman, C. Nicholson, Experimental optimization of current source-density technique for anuran cerebellum. *J. Neurophysiol.* **38**, 369–382 (1975).

42. T. Goto, *et al.*, An Evaluation of the Conductivity Profile in the Somatosensory Barrel Cortex of Wistar Rats. *J. Neurophysiol.* **104**, 3388–3412 (2010).

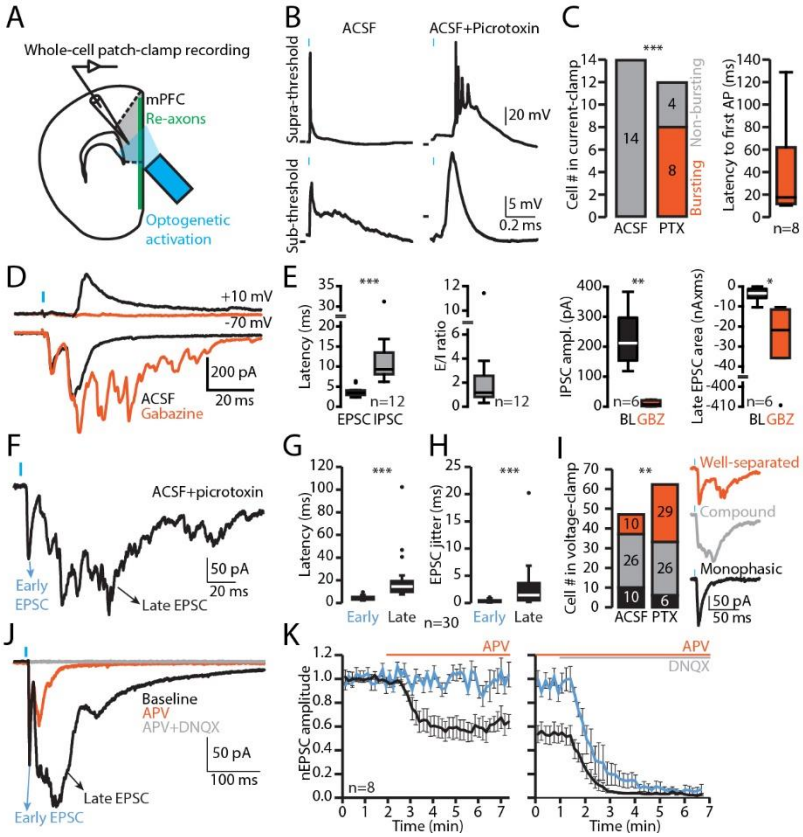

Figure 1. Re activation induces biphasic excitation in mPFC neurons. (A) Experimental approach: whole-cell patch-clamp recording of mPFC neurons combined with optogenetic stimulation of Re axons. (B) Example traces of EPSPs recorded in current-clamp mode around the resting membrane potential of the cell. Top and bottom traces show suprathreshold and subthreshold responses, respectively. Left: ACSF. Right: picrotoxin. Horizontal lines indicate -65 mV. (C) Left, bar graphs showing the number of bursting (orange) and non-bursting (grey) mPFC neurons upon light activation of Re afferents in ACSF and picrotoxin. Right, box-and-whisker plot of the latency from light stimulation to the peak of the first action potential in the delayed burst. (D) Example light evoked EPSC recorded at -70 mV (bottom) and IPSC recorded at +10 mV (top) in ACSF (black) and in gabazine (orange). Note the presence of two EPSCs, one early within 5ms of light stimulus, and a late compound EPSC, after a delay of about 10-15 ms. (E) From left to right, box-and-whisker plots of the EPSC and IPSC latencies from light onset, excitation/inhibition (E/I) ratio, IPSC amplitude in ACSF (black) and gabazine (orange), area of the late EPSC in ACSF (black) and gabazine (orange). (F) Example EPSC recorded at -70 mV with picrotoxin showing a late component with inflexions and notches. (G) Box-and-whisker plots of the latency of the early (blue) and late (black) components of the EPSCs from the light onset. (H) Same as B for EPSC jitter. (I) Bar graphs showing the number of monophasic EPSCs (black), compound EPSCS (grey) and evoked responses with a well-separated late EPSC (orange) in ACSF (left) and PTX (right). The inset shows 3 example EPSCs. (J) Example traces of EPSCs recorded at -70 mV in baseline condition (black) and after APV (orange) and DNQX (grey) bath application. (K) Graphical representation of the effect of APV (left) and DNQX (right) on the amplitude of the early (blue) and late (black) components of the EPSC. The EPSC amplitude was normalized to the amplitude during the baseline. Significance: * $p < 0.05$, ** $p < 0.01$, and *** $p < 0.001$.

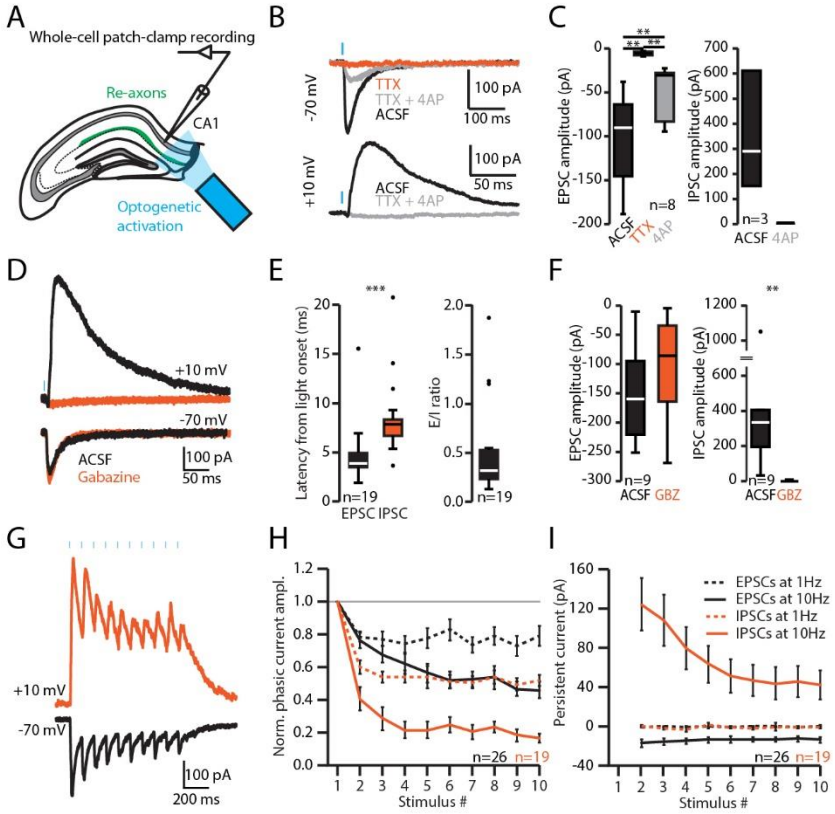

Figure 2. Re activation does not induce biphasic excitation in dCA1 pyramidal cells. (A) Scheme showing the whole-cell patch-clamp recording of dCA1 pyramidal neurons combined with optogenetic stimulation of Re axons. (B) Top, example traces of an EPSC evoked in a dCA1 pyramidal cell by Re activation in baseline condition (black), after TTX (orange) and 4AP (grey) bath application. Bottom, same for an IPSC in baseline condition (black) and after TTX+4AP (grey). (C) Left, EPSCs amplitude in baseline condition (black), in TTX (orange) and in 4AP (grey). Right, same for IPSCs. (D) Typical trace of an EPSC recorded at -70 mV (bottom) and of an IPSC recorded at +10 mV (top) in ACSF (black) and in gabazine (orange). (E) EPSCs and IPSCs latencies from the light onset and the E/I ratio. (F) Left, EPSC amplitude in ACSF (black) and gabazine (orange). Right, same for IPSC amplitude. (G) Example traces of the current responses of a dCA1 pyramidal cell upon a train of 10 light stimulations at 10 Hz of Re afferents at -70 mV (bottom, black) and at +10 mV (top, orange). (H) Peak amplitude of phasic PSC component for EPSCs (black) and IPSCs (orange) along the train of stimulation at 1 Hz (dashed lines) and at 10 Hz (continuous lines). Phasic current amplitudes are normalized to the amplitude of the first current response in the train. (I) Amplitude of persistent currents of the EPSCs (black) and IPSCs (orange) during a 1 Hz (dashed lines) and a 10 Hz (continuous lines) train of stimulation. Significance: * $p < 0.05$, ** $p < 0.01$, and *** $p < 0.001$.

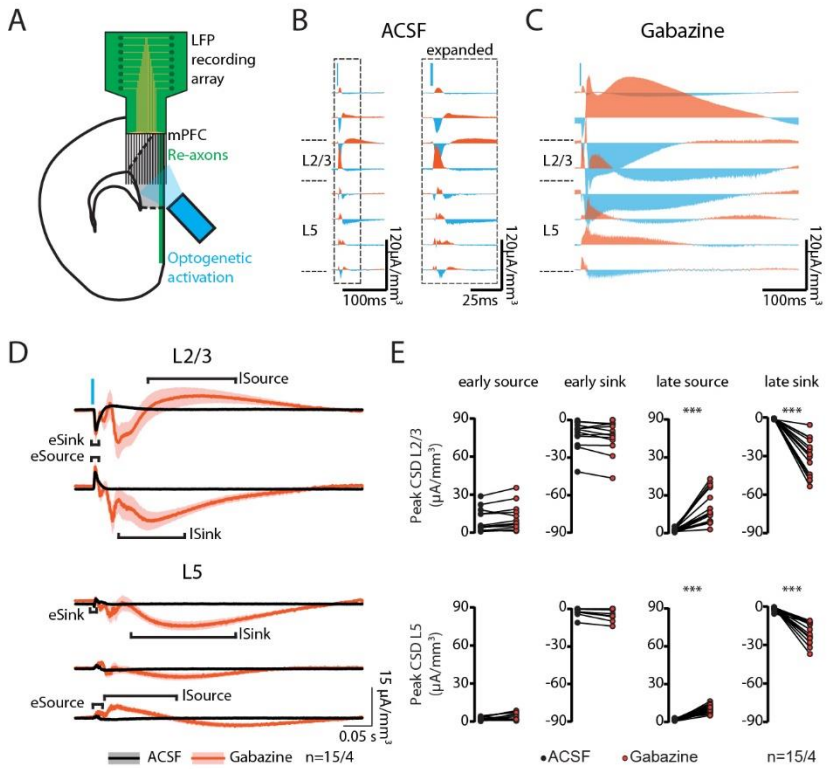

Figure 3. GABA$_A$R blockade reveals the delayed activation of mPFC local network upon Re activation. A) Experimental design of LFP recording in mPFC and optogenetic stimulation of Re axons. (B) Left, representative current source density (CSD) derived from the LFP recording. Right, same traces expanded in time. (C) Same as in (B) after gabazine application. Note the delayed, long-lasting increase in CSD signal in both upper and deep layers. (D) Average response of the postsynaptic sinks and sources in ACSF (black) and gabazine (orange) from 15 slices collected from 4 mice. Brackets highlight the traces used for quantification. (E) Graphs of the peak amplitude of CSD in upper (top) and deep (bottom) layers in ACSF (black) and gabazine (orange). The peak of early sinks and sources were measured 2 to 10 ms after the light onset. The peak of late sinks and sources were measured beyond 10 ms after the light onset. Significance: * $p < 0.05$, ** $p < 0.01$, and *** $p < 0.001$.

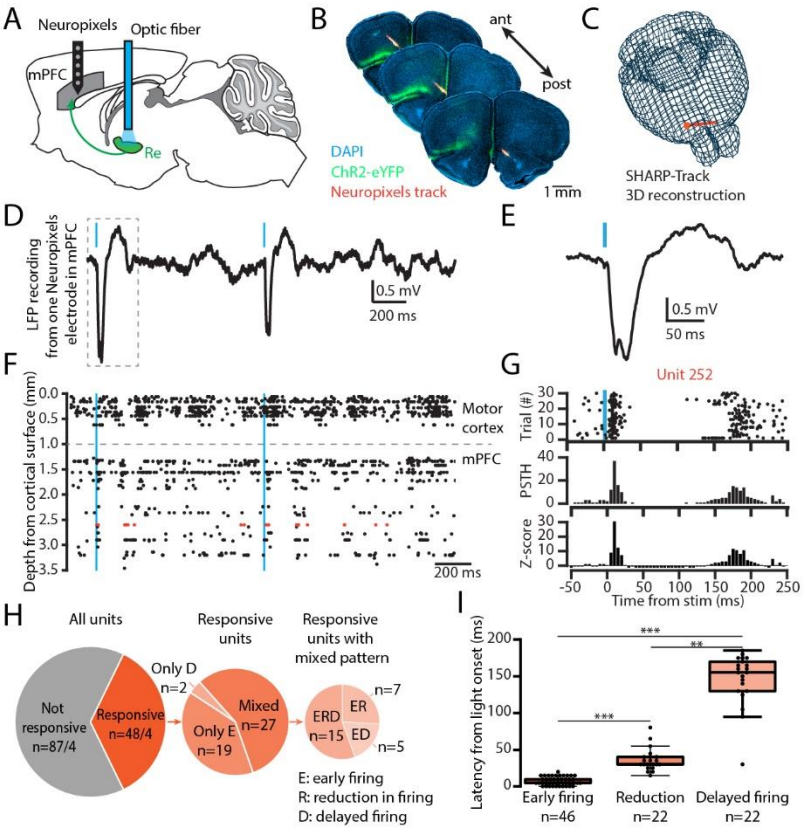

Figure 4. Activation of Re leads to biphasic excitation of mPFC units in vivo. (A) Scheme showing the Neuropixels recording of mPFC and motor related areas combined with optogenetic stimulation of Re axons. (B) Sequence of epifluorescent micrographs of coronal brain slices through mPFC of a mouse implanted with a Neuropixels probe. The track of the Neuropixels probe is labeled in red. Blue: DAPI staining. Green: ChR2-eYFP axons from the Re. (C) Representation of the Neuropixels probe track through the motor areas and mPFC reconstructed with Allen CCF tools (The Cortical Processing Laboratory at UCL). (D) Example trace of local field potential recording in mPFC upon optogenetic stimulation of Re. (E) Expanded trace from D. (F) Raster of 94 units firing during a 2 s long recording. Units are organized by their relative position from the probe tip. Vertical blue lines indicate two stimulations of the Re nucleus. (G) Raster plot, cumulative histogram, and Z-score analysis from an example unit responding to a 5 ms blue light activation of Re. (H) Proportion of units in mPFC responding to activation of Re and their pattern of firing. (I) Latencies from the light stimulation onset to each of the three distinct firing phases. Significance: * $p < 0.05$, ** $p < 0.01$, and *** $p < 0.001$.